Peer-reviewed version available at Atoms 2018, 6, 29; doi:10.3390/atoms6020029

Article

H-β line in a corona helium plasma: a multi-code line shape comparison

Roshin Raj Sheeba[1,*], Mohammed Koubiti[1], Nelly Bonifaci[2], Franck Gilleron[3], Caroline Mossé[1], Jean-Christophe Pain[3], Joël Rosato[1] and Evgeny Stambulchik[4]

1 Aix Marseille Univ, CNRS, PIIM, Marseille, France
2 Laboratoire G2Elab, CNRS/Grenoble University, 25 rue des Martyrs, 38042 Grenoble, France
3 CEA DAM, DIF, F-91297 Arpajon, France
4 Faculty of Physics, Weizmann Institute of Science, Rehovot 7610001, Israel

* Correspondence: roshin-raj.SHEEBA@univ-amu.fr

Abstract: Many spectroscopic diagnostics are routinely used as a technique to infer the plasma parameters from line emission spectra but their accuracy depends on the numerical model or code used for the fitting process. However, the validation of a line shape code requires some steps : comparison of the line shape code with other similar codes for some academic (simple) cases and then more complex ones, comparison of the fitting parameters obtained from the best fit of the experimental spectra with those obtained with other diagnostic techniques and/or comparison of the fitting parameters obtained by different codes to fit the same experimental data. Here we compare the profiles of the hydrogen Balmer β line in a helium plasma computed by six codes for a selected set of plasma parameters and we report on the plasma parameters inferred by each of them from the fitting to a number of experimental spectra measured in a helium corona discharge where the pressure was in the range 1- 5 bar.

Keywords: Stark broadening; van der Waals broadening; Line shapes; Helium plasma; Corona discharge; Plasma diagnostics; Code comparison; Neutral broadening; Pressure broadening

1. Introduction

Spectra of lines emitted in gases and plasmas are routinely used as a diagnostic technique to infer the plasma parameters such as the electron density and temperature depending on the emitter environment and the different broadening mechanisms. Obviously the accuracy of the deduced parameters depends on that of the line shape code used to fit the experimental data. It is therefore mandatory to check the validity of any line shape code before using it for diagnostic purposes. The series of international workshops on Spectral Line Shapes in Plasmas [1] is a unique opportunity allowing all line shape code developers to cross check their codes (numerical models and/or simulations). Generally speaking, to validate a line shape code, one has to realize the following tasks or steps: compare the line shape code with other similar codes for some academic (simple) cases and then for more complex ones, fit an experimental emission spectrum and compare the deduced parameters corresponding to the best fit with those obtained with other independent diagnostic techniques if available and/or compare the inferred parameters from the fitting attempts using different codes to fit the same experimental spectrum. During the last edition of this workshop series, i.e., SLSP4 [2], many cases were proposed for line shape code comparison and some of them are the subject of papers published in this issue. In the category of the challenging case consisting to confront the codes to a real situation, it was proposed to analyze two lines emitted in a helium corona discharge where the pressure was increased from 1 to 5 bars. These are the hydrogen Balmer-β (486 nm) and He I 492 nm lines measured simultaneously from the same plasma. The participants were asked to fit both lines in order to get consistent plasma parameters. However, as the two lines were

fitted independently and knowing that the major effort was focused on the Hydrogen Balmer-β line with the contributions of five codes against while only the experimental data for the lowest pressures were considered for the He I 492 nm by up to four codes, we have decided to limit this paper to the hydrogen Balmer-β line. The helium He I 492 nm line is a subject of another but shorter paper in this same issue. Therefore, here we compare the profiles of the H-β line in a helium plasma computed by five codes for a selected set of plasma parameters and we report on the plasma parameters inferred by each of them from the fitting to a number of experimental spectra measured in a helium corona discharge where the pressure was in the range 1- 5 bar.

This paper is divided in two parts. The first part is devoted to the synthetic profiles of the H-β line emitted by hydrogen atoms perturbed by the electrons and He^+ ions of a helium plasma. The second part is focused on comparison with experimental spectra of the same line measured in a corona discharge in helium. The aim in the first part was to compare the pure Stark-broadened profiles of this line calculated by the contributing codes for a selected set of plasma parameters. The latter, assumed to correspond to conditions of a corona discharge in helium, are the following: two values for the electron density $n_e=10^{15}$ and 10^{16} cm^{-3}, three values for the electron and ion temperatures assumed to be equal: $T_e=T_i=0.1$, 0.2 and 0.4 eV. The choice to retain only the Stark broadening is aimed to highlight the differences between the participating codes and is justified by the fact that other broadening mechanisms are less important even though not completely negligible. Indeed, as we will see in the section devoted to the data fitting, Doppler and van der Waals broadenings have to be included as well as the instrumental function. The van der Waals broadening, which is a due to the interactions of the hydrogen atoms with neutral helium atoms present in the partially ionized helium plasma, is roughly comparable to the Doppler broadening unlike resonance broadening which is due the interactions of neutral emitters with neutrals of the same species.

2. Brief description of the codes

This section describes briefly the different codes contributing to this case study (termed case 14). Five codes were involved: two simulation methods and three models. The simulation codes are LSNS and SimU. LSNS involves a numerical integration of the time-dependent Schrödinger equation for the hydrogen wave function under the influence of a fluctuating electric field obtained from a particle simulation. More details can be found in [3] and references therein. SimU is well described in [4-5]. The three models are PPP [6], QC_FFM ([7] and the references therein) and ZEST. Since ZEST (ZEeman-STark) line-shape code has been improved and upgraded to a new version [8], we describe here the version that has been used for the calculations reported in this paper. ZEST relies on a quasi-static description of the ions and an impact approximation for the electrons. The Hamiltonian of the radiator includes Stark effect in the dipole approximation for arbitrary multi-electron ions as well as Zeeman effect accounting for a static magnetic field. The impact of the magnetic field on the electron trajectories is not taken into account. The electrons are described by a collision operator calculated up to the second order of the electron-radiator interaction using the model of R.W. Lee [9]. The distribution of quasi-static ion fields is evaluated using analytical formulas adjusted on many Monte-Carlo simulations as a function of the plasma ion coupling parameter and the effective electron-ion screening parameter [10-11]. At the time of calculations, ZEST neglected the collisional shift due to the electrons, the interference terms between upper and lower states, the non-diagonal terms of the collision operator and the frequency dependence of the impact width. Using the unitary transformation that diagonalizes the radiator Hamiltonian, the resulting profile is then written as a sum of Lorentzian functions (or Voigt functions when accounting for Doppler effect) weighted by the strength of the Stark components and by the probability of the quasi-static ion fields. All the time of

the calculations presented here, the ZEST code did not include the ion dynamics effects. Now, in the most recent version of ZEST [8], the ion dynamics effects are modeled within the framework of the fast Frequency-Fluctuation Model (fast FFM) [12]. In the next section, we compare the calculated profiles and the widths at half-maximum for the two densities (lower density $n_e=10^{15}$ cm^{-3}) and higher density ($n_e=10^{16}$ cm^{-3}).

3. Code comparison through profiles and line widths

3.1. *H-β line profiles for the lower density*

The results of the code calculations for the lower density case ($n_e=10^{15}$ cm^{-3}) are respectively illustrated for equal ion and electron temperatures of 0.1, 0.2 and 0.4 eV in Figures 1-3. It can be seen that all the codes except PPP are in an overall agreement in terms of widths and line shapes with some differences in the central line dip. The profiles calculated by PPP are broader than all other especially at the lowest temperature of 0.1 eV. This was excepted because this version of the PPP line shape code used for the treatment of the electron broadening the GBK (Griem-Blaha-Kepple) [13] collision operator which does not depend on the frequency. This operator is known to overestimate the broadening in comparison to frequency dependent collision operators in the framework of the impact approximation used for the treatment of the emitter-electron interactions. Note that in ZEST calculations, the electron broadening was treated using Lee's model in the impact limit. Such an operator is different from the GBK one used in PPP, but does not account for frequency dependence either. Note that LSNS has been applied to the spectrum corresponding to the lowest pressure in a separate study [23]. The calculations of the PPP code tends towards the other code calculations as the temperature increases from 0.1 to 0.4 eV. At 0.4 eV, all the profiles give close widths even though they differ in the filling of the line center dip.

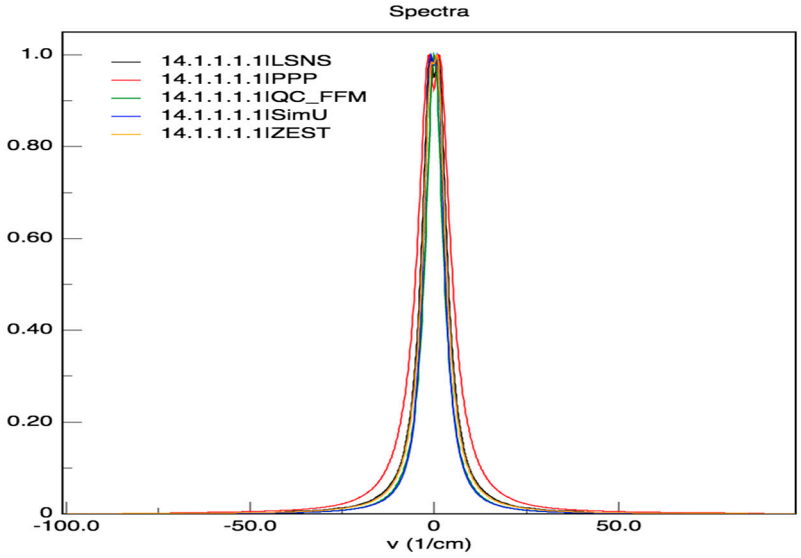

Figure 1. Theoretical Stark profiles of the H-β line calculated for hydrogen atoms in a helium plasma with an electron density of 10^{15} cm^{-3} and a temperature of 0.1 eV for both plasma He^+ ions and electrons. The profiles are centered at 486.1 nm and wavenumber units are used. Solid black: LSNS, red: PPP, green: QC_FFM, blue: SimU, yellow: ZEST.

Preprints (www.preprints.org) | NOT PEER-REVIEWED | Posted: 6 March 2018 doi:10.20944/preprints201803.0040.v1

Peer-reviewed version available at Atoms 2018, 6, 29; doi:10.3390/atoms6020029

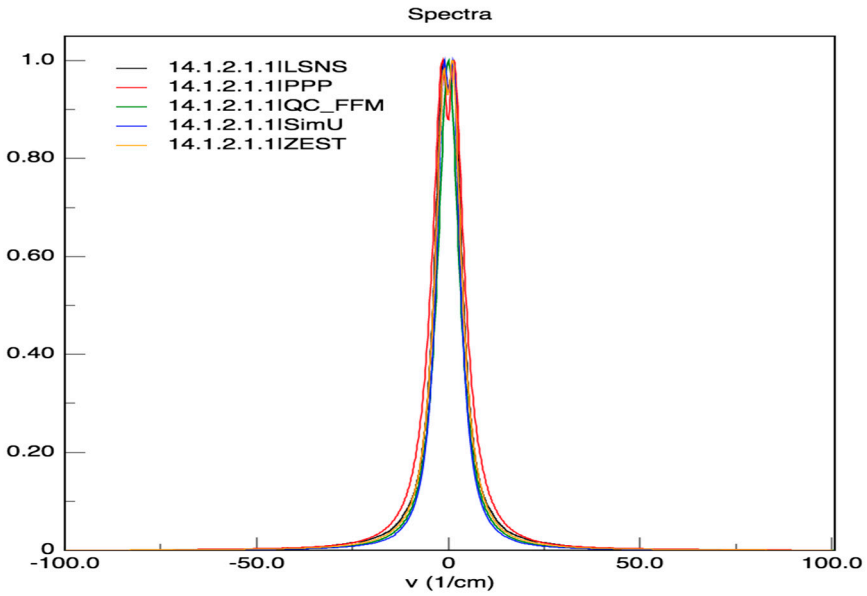

Figure 2. Same as Figure 1 but for T_e=T_i=0.2 eV. Same line styles and code colors as Figure 1.

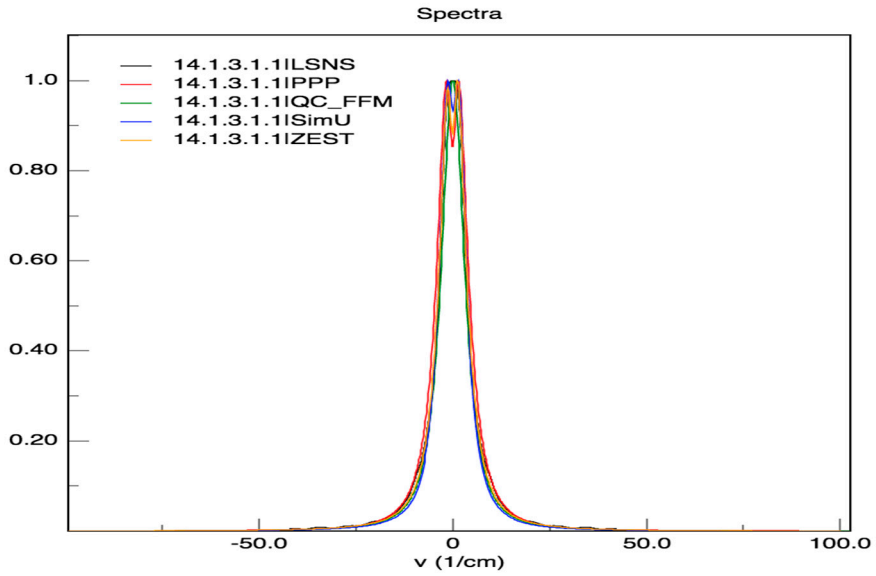

Figure 3. Same as Figures 1 and 2 with the same line styles and code colors but for T_e=T_i=0.4 eV.

3.2. H-β line profiles for the highest density

Similarly, the results of the code calculations for the higher density case (n_e=10^{16} cm^{-3}) and the same temperatures as in the previous subsection are respectively illustrated in Figures 4-6. For this density, the expected discrepancy between the calculations carried out by the PPP code using the GBK collision operator and those of the other codes are more pronounced confirming the non-validity of this form of this operator at high densities and low temperatures even though it tends to disappear with increasing temperatures. One can see that for the remaining calculations, SimU agrees well with QC_FFM on the one side and ZEST agrees well with LSNS on the other side. Note that the profiles calculated by LSNS and ZEST are a bit broader than those calculated by SimU and QC_FFM. These

Preprints (www.preprints.org) | NOT PEER-REVIEWED | Posted: 6 March 2018 doi:10.20944/preprints201803.0040.v1

Peer-reviewed version available at Atoms 2018, 6, 29; doi:10.3390/atoms6020029

agreements concern the overall profiles, the line widths and wings but not the line center dip for which there are some discrepancies between the various code calculations.

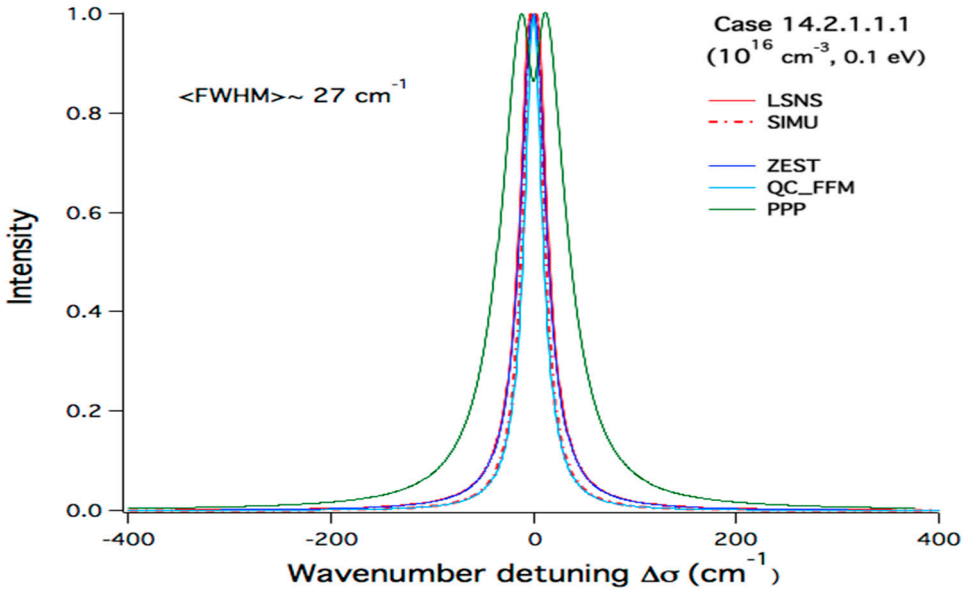

Figure 4. Theoretical Stark profiles of the H-β line calculated for hydrogen atoms in a helium plasma with an electron density of 10^{16} cm^{-3} and a temperature of 0.1 eV for both plasma He^+ ions and electrons. The profiles are centered at 486.1 nm and wavenumber units are used. Solid red: LSNS, solid blue: ZEST, solid light blue: QC_FFM, olive green: PPP, dot-dashed red: SimU.

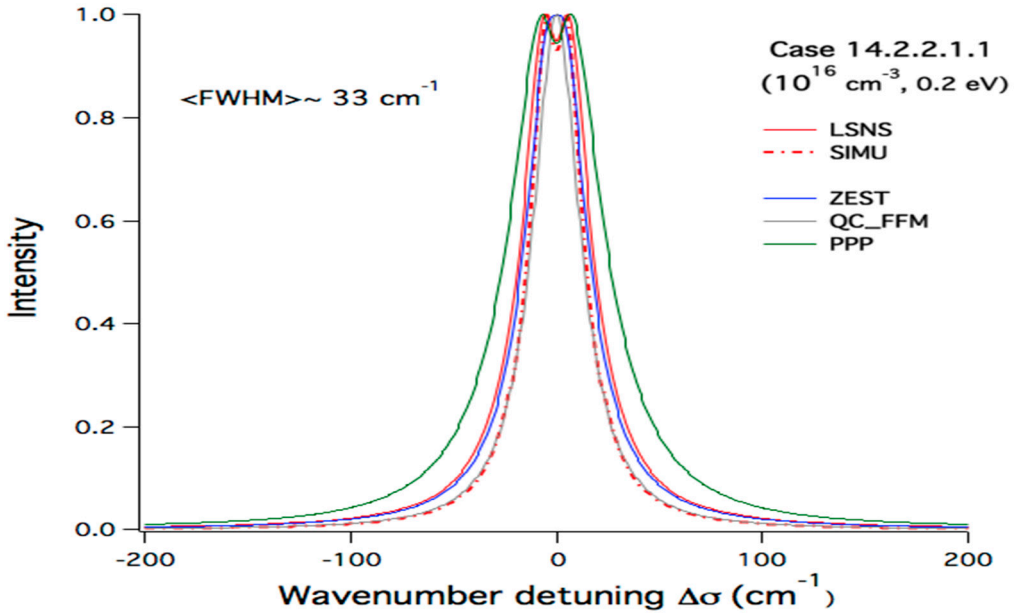

Figure 5. Same as Figure 4 but for T_e=T_i=0.2 eV. Same line styles and code colors as Figure 4.

Preprints (www.preprints.org) | NOT PEER-REVIEWED | Posted: 6 March 2018 doi:10.20944/preprints201803.0040.v1

Peer-reviewed version available at Atoms 2018, 6, 29; doi:10.3390/atoms6020029

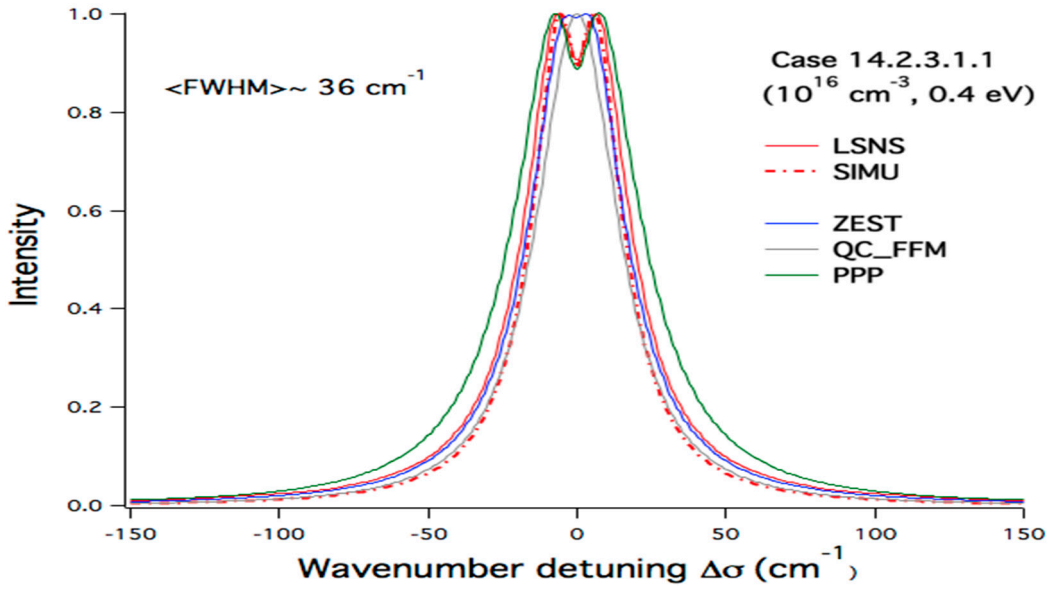

Figure 6. Same as Figures 4 and 5 with the same line styles and code colors but for T_e=T_i=0.4 eV.

3.3. *Comparison of the FWHM of the H-β line*

The FWHM (Full Widths at Half Maximum) of the H-β line vs the electron temperature (0.1, 0.2 and 0.4 eV) as calculated by the previously mentioned codes are illustrated on Figure 7 for both electron densities, i.e., n_e=10^{15} and 10^{16} cm^{-3}. This figure shows the relative dispersion of the FWHM as deduced from the codes when those of PPP are higher especially at the highest density and lowest temperature. More details are shown in Table 1.

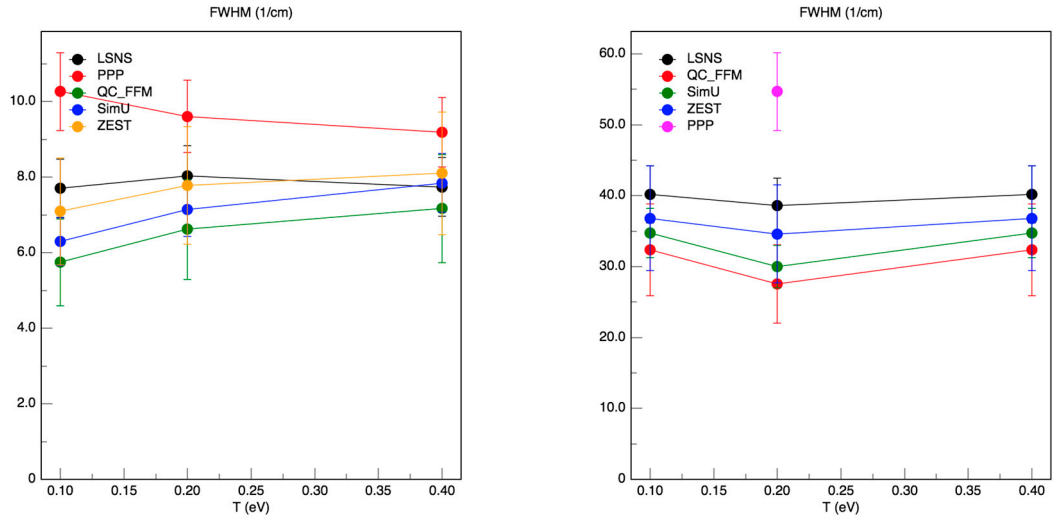

(**a**) (**b**)

Figure 7. The H-β line Full Widths at Half Maximum (FWHM) versus the electron temperature as deduced from the profiles calculated by the codes. (**a**) Lower electron density (n_e=10^{15} cm^{-3}). (**b**) Higher electron density (n_e=10^{16} cm^{-3}).

In Table 1, the FWHM for each subcase corresponding to a couple of n_e, T_e, are presented as well as the ratio of the highest value of the FWHM to each FWHM value. In addition, the mean value of the FWHM is calculated using all the values but the highest. For instance for the lowest density, the mean value <FWHM> of the FWHM varies between 5.75 cm^{-1} for 0.1 eV to ~7.7 cm^{-1} for 0.4 eV.

Roughly the FWHM values of the profiles calculated by PPP are about 1.2-1.5 higher than the average values. For the highest density, the mean value of the FWHM (excluding the highest value) is in the range 27-36 cm^{-1}, with the lower value (27 cm^{-1}) corresponding to the lowest temperature, i.e., 0.1 eV. As explained previously, the FWHM calculated by PPP are higher than those of the other codes. It is about 2.8 times the mean value for 0.1 eV and decreases down to be 1.7 times higher at 0.2 eV to becomes eventually equal to the mean value at temperatures of 0.4 eV or higher leading to a very good agreement with the other codes. This means that the calculations done by PPP using the non-frequency depending collision operator can be safely used for comparisons with the experimental data provided that the temperatures are not too low and the density too high.

Table 1. FWHM in units of cm^{-1} as deduced from the profiles calculated by each of the five codes LSNS, PPP, C_FFM, SimU and ZEST. The FWHM ratio stands for the ratio of the highest value of the FWHM to each FWHM. The highest value corresponds to the PPP calculations except for $n_e=10^{16}$ cm^{-3} and T_e=0.4 eV where its corresponds to LSNS calculations.

Plasma Parameters	Codes				
	LSNS	**PPP**	**QC_FFM**	**SimU**	**ZEST**
$n_e=10^{15}$ cm^{-3}, $T_e=T_i$=0.1 eV					
FWHM (cm^{-1})	7.71	10.26	5.75	6.29	7.09
FWHM ratio	1.3	1.0	1.8	1.6	1.4
$n_e=10^{15}$ cm^{-3}, $T_e=T_i$=0.2 eV					
FWHM (cm^{-1})	8.03	9.61	6.62	7.15	7.78
FWHM ratio	1.2	1.0	1.4	1.3	1.2
$n_e=10^{15}$ cm^{-3}, $T_e=T_i$=0.4 eV					
FWHM (cm^{-1})	7.74	9.19	7.17	7.85	8.10
FWHM ratio	1.2	1.0	1.3	1.2	1.1
$n_e=10^{16}$ cm^{-3}, $T_e=T_i$=0.1 eV					
FWHM (cm^{-1})	32.24	73.00	21.27	24.40	30.00
FWHM ratio	2.3	1.0	3.4	3.0	2.4
$n_e=10^{16}$ cm^{-3}, $T_e=T_i$=0.2 eV					
FWHM (cm^{-1})	38.59	54.67	27.56	29.98	34.60
FWHM ratio	1.4	1.0	2.0	1.8	1.6
$n_e=10^{16}$ cm^{-3}, $T_e=T_i$=0.4 eV					
FWHM (cm^{-1})	40.18	36.00	32.34	34.73	36.82
FWHM ratio[1]	1.0	1.1	1.2	1.2	1.1

[1] The highest value of the FWHM for this case corresponds to LSNS. It corresponds to PPP for all other considered cases.

3.4. Reconsidering the PPP of the H-β line

Following the previous discussion on the comparisons of profiles and trying to take advantage from the detailed comparisons of the H-β line widths presented in Table 1, we have recalculated the profiles using the PPP code for each of the six subcases by dividing

Preprints (www.preprints.org) | NOT PEER-REVIEWED | Posted: 6 March 2018 doi:10.20944/preprints201803.0040.v1

Peer-reviewed version available at Atoms 2018, 6, 29; doi:10.3390/atoms6020029

the electron density by the corresponding factor mentioned at the end of the previous subsection. These calculations have been termed PPPm. They are shown on Figures 8 and 9 for the lowest density. In figure 8, a semi-logarithmic scale has been used. It can be seen from both graphs, the reduction of electron density by the correct factor allows the PPP calculations termed PPPm to approach closely the other calculations in terms of line widths and wings but introduces differences in the line center dip which becomes more pronounced with PPPm. Therefore, this artificial way to reduce the overestimated broadening due to the GBK collision operator works roughly and therefore, one has to use a frequency-dependent collision operator especially for low temperatures and high densities.

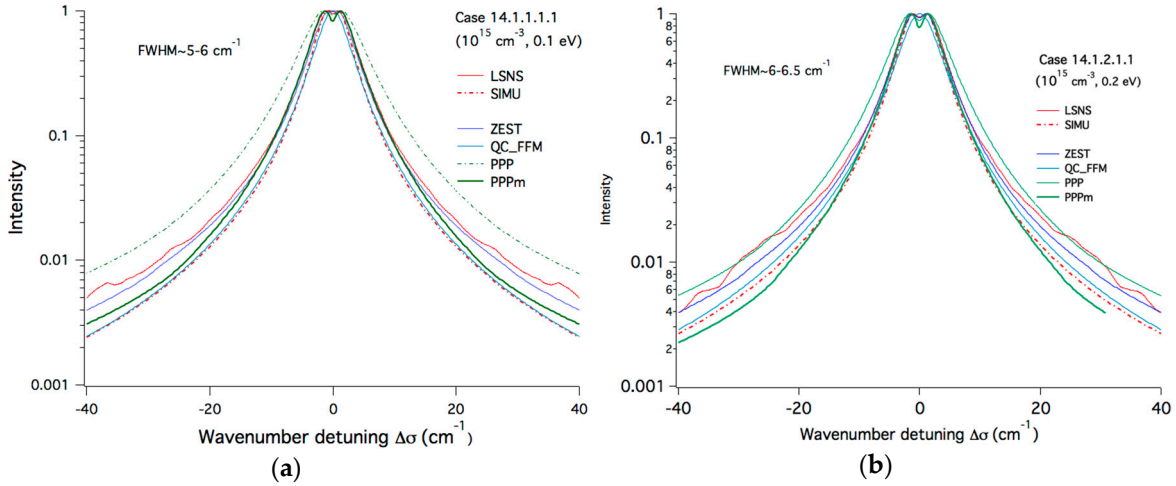

Figure 8. Theoretical Stark profiles of the H-β line of figures 1 and 2 with the inclusion of modified PPP calculations (PPPm : thick green solid line) where the electron density was scaled down by the mean corresponding factor explained at the end of subsection **3.3**. The same factor of 1.5 was used for both subcases (**a**) T_e=T_i=0.1 eV (**b**) T_e=T_i=0.2 eV.

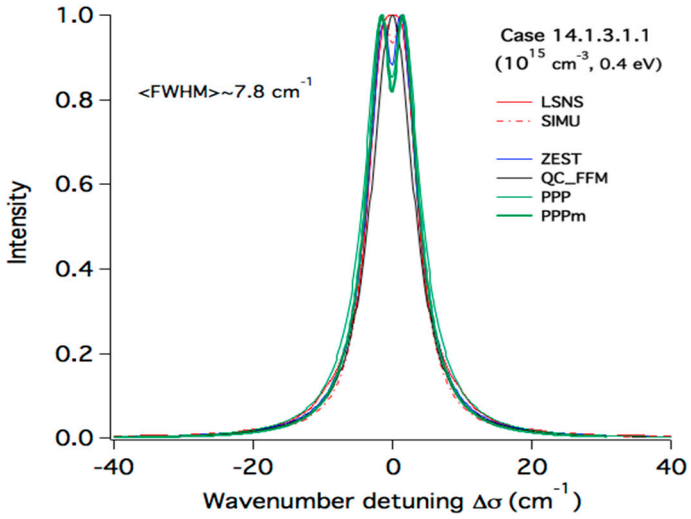

Figure 9. Theoretical Stark profiles of the H-β line of figure 3 (T_e=T_i=0.4 eV) with the inclusion of modified PPP calculations (PPPm : thick green solid line) where the electron density was scaled down by the mean corresponding factor explained at the end of subsection **3.3**. The factor used here is 1.2

3.5. *Electric microfield distributions*

To be complete in the code comparisons and for a better understanding of the differences between the calculated profiles, we present on Figure 10 for the lowest density ne=10^{15} cm^{-3}, the field distribution used by the codes except QC_FFM. One can see no difference between the distributions calculated by LSNS, PPP and ZEST. As SimU simulates both electrons and ions providing the total electric field, it is normal that its field distribution shown is broader and shifted towards higher field values. For the other codes, the field distributions shown here are for ions only.

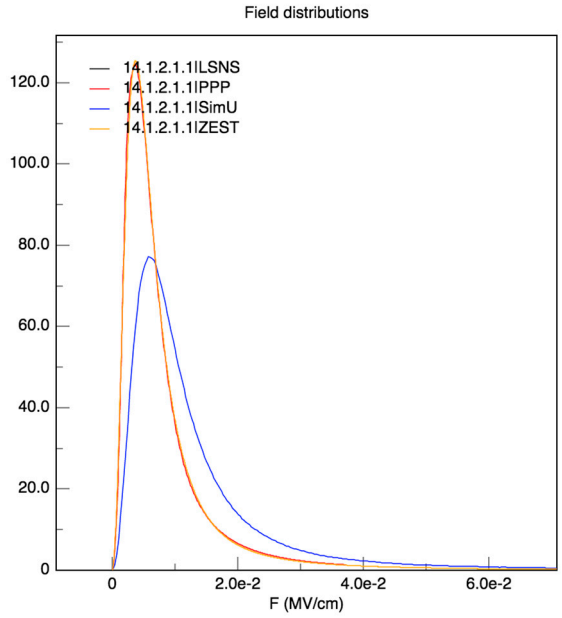

Figure 10. Ion electric field distribution as calculated by the different line shape codes except QC_FFM. It corresponds to the lowest electron density of $n_e=10^{15}$ cm^{-3} and $T_e=T_i=0.1$ eV.

4. Comparison with experimental spectra: line shape fitting

4.1. *Introducing the experimental spectra*

The experimental spectra proposed as a best-fit challenge for the codes here were measured in a corona discharge in helium performed in an electrical engineering laboratory for the study of the dielectric properties of insulators [14-15]. Spectra of the H-β line were measured at the room temperature for various values of the pressure. Spectra corresponding to six values of the pressure in the range 1-5 bars are shown in Figure 11. The spectra corresponding to the pressure values of 1, 1.5, 2, 3, 4 and 5 bars were respectively labeled 14a, 14b, 14c, 14d, 14e and 14f. Before presenting the fitting results of these spectra, it is necessary to give some insights into the broadening mechanisms affecting the H-β line emitted in a helium plasma in which hydrogen atoms represent a small fraction of the environment.

Preprints (www.preprints.org) | NOT PEER-REVIEWED | Posted: 6 March 2018 doi:10.20944/preprints201803.0040.v1

Peer-reviewed version available at Atoms 2018, 6, 29; doi:10.3390/atoms6020029

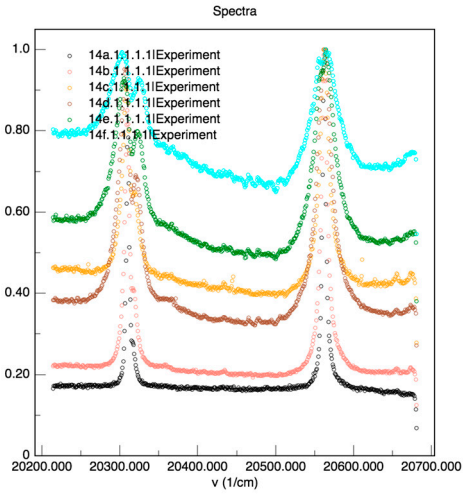

Figure 11. Superposition of six experimental spectra of the H-β 486.1 nm (right peak) and the helium He I 492 nm (left peak) lines measured at the room temperature for pressures varying between 1 bar (bottom : black line) to 5 bars (top: light blue). Red, dark brown, light brown and green lines correspond to pressures of 1.5, 2, 3 and 4 bars respectively. Spectra are labelled 14a (P=1 bar) to 14f (P=5 bars).

4.2. Broadening mechanisms of H-β line in a helium plasma

The experimental spectral shapes of the H-β line emitted by a corona discharge in helium with hydrogen traces are subject to a competition between several broadening mechanisms. First of all, the natural broadening is intrinsic to each emitter but is very small in comparison to other mechanisms. There is also another unavoidable contribution from the instrumental function mainly due to the spectrometer entrance slit. For the present case, the instrumental function has been estimated from a helium lamp as a Gaussian with a FWHM less than 0.01 nm [15]. Four other broadening mechanisms can potentially contribute to the line profile of the H-β line. Three of these mechanisms depend mainly on the temperature: Doppler broadening, resonance and van der Waals broadenings. The fourth broadening mechanism that depends on the electron density is the Stark broadening. Resonance broadening is due to collisions of hydrogen atoms with other hydrogen atoms, it leads to a Lorentzian profile with a FWHM proportional to the ratio (P/T) of the pressure over the temperature of the hydrogen atoms i.e., $\Delta\lambda_{res} \propto (P/T)$ with a linear dependence on the fraction of the hydrogen atoms in the helium plasma. van der Waals broadening is attributed to collisions of the hydrogen atoms with other neutrals which are connected to the emitter through a resonant transition. It is the case for the interactions of the hydrogen atoms with helium neutrals. Like resonance broadening, the van der Waals broadening mechanism results in a Lorentzian shape with FWHM $\Delta\lambda_{VdW}$ proportional to the pressure P and inversely proportional to the power 0.7 of the temperature i.e.$\Delta\lambda_{VdW} \propto \left(\frac{P}{T^{0.7}}\right)$. Readers interested in these kinds of pressure broadening mechanisms between neutral atoms can refer for instance to the following papers [16-21]. In all the fitting presented here, the resonance broadening was estimated to be negligible in comparison to other broadening mechanisms and was therefore ignored and this can be easily justified in particular for low concentrations or fractions of neutral hydrogen atoms. We have estimated the van der Waals broadening FWHM for each of the six experimental spectra. These are tabulated on Table 2 and compared to the corresponding FWHM of the experimental spectra. It can be seen that the van der Waals broadening represents about one third of the total broadening of the H-β line, the remaining broadening being due mainly to Stark effect and to Doppler effect to some extent.

Preprints (www.preprints.org) | NOT PEER-REVIEWED | Posted: 6 March 2018 doi:10.20944/preprints201803.0040.v1

Peer-reviewed version available at Atoms 2018, 6, 29; doi:10.3390/atoms6020029

Table 2. Summary of the FWHM of the van der Waals broadening compared with the experimental FWHM of the six experimental spectra of the H-β line in a helium plasma considered in this paper.

Pressure (bars)	$\Delta\lambda_{VdW}$(nm)	$\Delta\lambda_{exp}$ (nm)	$\Delta\lambda_{VdW}/\Delta\lambda_{exp}$(%)
1	0.051	0.143	35
1.5	0.076	0.206	36
2	0.101	0.335	30
3	0.152	0.510	30
4	0.202	0.604	31
5	0.253	0.819	31

4.3. Comparison with experimental data: spectral fitting

We have arbitrarily classified the six spectra in three categories: low pressure consisting of the two lower pressure cases 14a and 14b, the intermediate pressure corresponding to pressures of 2 and 3 bars (cases 14c and 14d) and high pressure for the highest pressure values 4 and 5 bars (cases 14e and 14f).

4.3.1. Cases of low pressure

The two spectra of these two low pressure values of 1 and 1.5 bars termed cases 14a and 14b were the most fitted with 6 attempts by 5 codes: LSNS, QC_FFM, ZEST, PPP and PPP_GC. PPP_GC is a fitting procedure based on the Genetic Algorithm interfaced with the PPP code. It is described in [22] where more recent fitting results of the H-β and He I 492 nm lines in the same conditions as those of this paper was fitted. PPP was used with two contributions numbered n°1 and n°2 differing only by the used parameters for the comparison with the experimental spectra. The fitted spectra are presented in Figure 12.

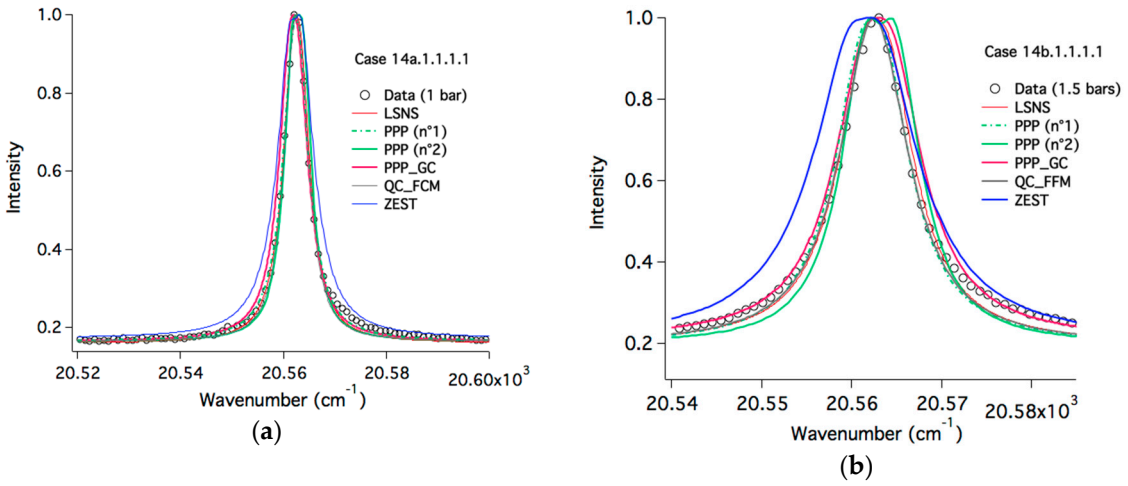

Figure 12. Comparison/fitting of the low pressure H-β spectra taking into account the Stark effect, the other broadening mechanisms like Doppler and van der Waals were not necessarily taken into account by all the codes. (**a**) P=1 bar (**b**) P=1.5 bars.

In figure 12, it can be seen that all the code attempts agree with the experimental data for both pressures except the calculations of ZEST. Deviations of the ZEST attempts increase with increasing

pressure. It is worth noting that the ZEST calculations tried to interpret the hydrogen H-β (486.1 nm) and the He I 492 nm lines at the same time, using the same plasma conditions. The difficulty to find such conditions for both lines may explain the disagreement observed on this particular line. A better agreement would have been obtained probably if the two lines had been fitted independently. More details on the fitting and the deduced parameters will be summarized in Table 3 for the entire set of spectra.

4.3.2. Cases of intermediate pressures

The two spectra of these two intermediate pressure values of 2 and 3 bars termed cases 14c and 14d were fitted by 4 attempts for case 14c and only three attempts for case 14d. For case 14c, three codes were used PPP (2 attempts), PPP_GC and QC_FFM while for case 14d only PPP (2 attempts) and QC_FFM were used. The fitted spectra are presented on Figure 13.

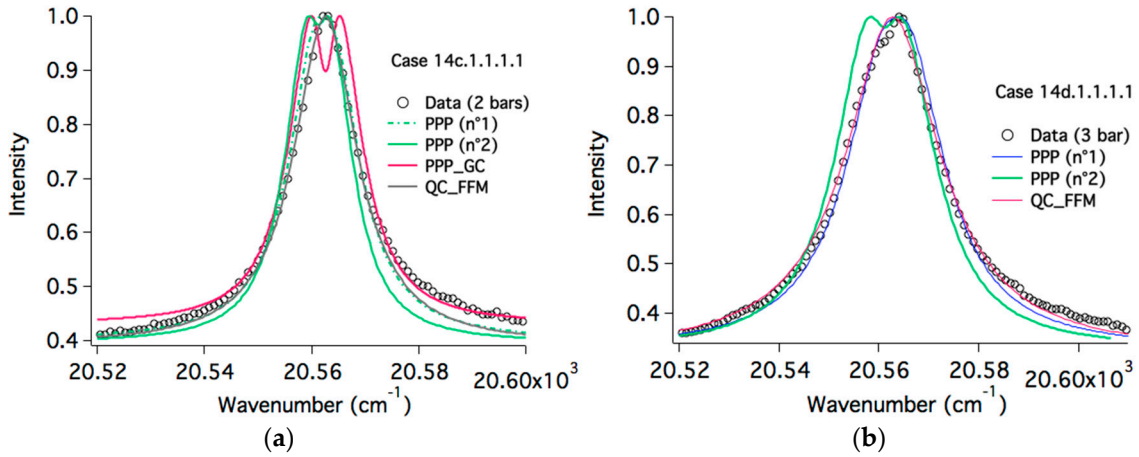

Figure 13. Comparison/fitting of the intermediate pressure H-β spectra. (**a**) P=2 bars (**b**) P=3 bars. The contributions are similar to those of Figure 12.

It can be seen from Figure 13 (a) that the data are well fitted by the PPP calculations (n°1 and n°2) and QC_FFM, the attempt of PPP_GC does not fit the spectrum. For case 14d illustrated on Figure 13 (b), one can see that both PPP (case n°2) and QC_FFM are able to reproduce the experimental spectrum. As indicated previously, the best parameters will be summarized in Table 3.

4.3.3. Cases of high pressures

The experimental spectra termed 14e and 14f corresponding to the "high pressure" category were compared to theoretical profiles calculated by only PPP and QC_FFM as shown on Figure 14. These spectra differ from the previous ones by their widths which is much larger and their asymmetry which can be clearly seen. These spectra are difficult to fit since they present some asymmetry in both around the line center and the line wings. If we ignore this and concentrate on the line widths, they are relatively well fitted by both codes QC_FFM and PPP. We will come back to the fitting parameters in the next section in particular in Table 3.

Preprints (www.preprints.org) | NOT PEER-REVIEWED | Posted: 6 March 2018 doi:10.20944/preprints201803.0040.v1

Peer-reviewed version available at Atoms 2018, 6, 29; doi:10.3390/atoms6020029

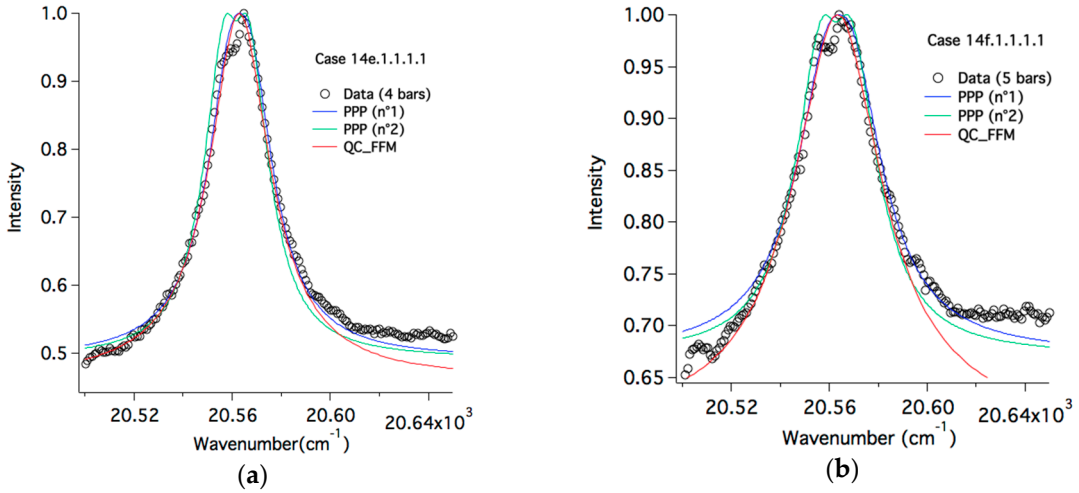

Figure 14. Comparison/fitting of the high pressure H-β spectra. (**a**) P=4 bars (**b**) P=5 bars. The contributions are similar to those of Figure 13.

4.4. Interpretation of the fitting parameters

Before summarizing the plasma parameters inferred from the fitting of the experimental spectra of the H-β line as measured in a corona discharge in helium at room temperature but at pressure in the range 1-5 bars, it is necessary to clarify the hypotheses and assumptions considered by each participant in the fitting or comparison with the experimental data. Data fitting with the LSNS code are based on: Stark broadening including dynamics effect, inclusion of the van der Waals broadening but no instrumental function. The temperatures were fixed as follows: equal emitter (T_a) and ion (T_i) temperatures (T_a=T_i=300 K), electron temperature (1 eV = 11604 K). The only free parameter was the electron density. Profiles calculated with PPP to fit the spectra were based on the following: Stark effect including ion dynamics, no instrumental function, inclusion of van der Waals broadening without (PPP n°1) and with Doppler broadening (PPP n°2). In both cases, the temperatures were fixed and only the electron density was allowed to vary. The fixed temperatures were as follows: T_a=T_i=T_e=300 K for PPP n°1 calculations and T_a=T_i=300 K and T_e=1 eV for PPP n°2 calculations. PPP_GC, Stark broadening was computed with the ion dynamics effect and the inclusion of Doppler and van der Waals broadenings without any instrumental function. The ion and neutral temperatures were assumed to be equal and fixed to 300K while allowing both the electron density and temperature to vary in prescribed domains. In QC_FFM calculations, in addition to the Stark broadening, the instrumental function and the Doppler broadening were added but not the van der Waals broadening. The temperatures were fixed T_i=T_a=0.1 eV; T_e=1 eV. ZEST calculations are based on the Stark broadening without the inclusion of ion dynamics neither the van der Waals broadening. The temperatures were: T_i=T_e=0.1 eV.

Table 3. Electron densities (in units of 10^{15} cm^{-3}) as inferred from the fit of the experimental H-β spectra by the contributing codes. P is the pressure in units of bars.

Case	P	LSNS	PPP (n°1)	PPP (n°2)	PPP_GC	QC_FFM	ZEST
14a	1	0.5	0.15	0.26	0.18	0.8	1.2
14b	1.5	1.1	0.3	0.58	0.38	2.2	2.7
14c	2	-	0.55	1.0	1.3	4.7	-
14d	3	-	0.9	2.0	-	10.0	-
14e	4	-	1.3	2.8	-	15.0	-
14f	5	-	1.9	3.8	-	27.0	-

5. Discussion and conclusion

Now we can present the results of the comparisons with the experimental data. For completeness, we have chosen to present them as a table in Table 3. The interpretation of these results is very difficult as they were determined using other parameters which have been fixed differently from one code to another. However, this does not prevent drawing some conclusions. For the lowest pressure case, the deduced electron densities are in the range $1.5x10^{14}$-$1.2x10^{15}$ cm^{-3}. If one looks in more details to the results, it can be seen that PPP n°1 and PPP_GC values are very close even though in PPP n°1 the Doppler broadening was not included and the electron temperature was only 300K while in PPP_GC, the Doppler effect was retained and the electron density was found to be ~1000 K. PPP n°2 calculations retaining Stark, Doppler and van der Waals broadening for an electron temperature of 1 eV gave an electron density of the same order of magnitude, i.e., $2.6x10^{14}$ cm^{-3}. For the same temperatures as those of PPP n°2 calculations and by retaining only Stark and van der Waals broadenings, the LSNS calculations gave a density about 2 times higher, i.e., $5x10^{14}$ cm^{-3}. The electron densities obtained by QC_FFM and ZEST were respectively $8x10^{14}$ and $1.2x10^{15}$ cm^{-3} for an electron temperature of 1 eV and 0.1 eV respectively. For the 1.5 bar case, similar results were obtained where the electron density values cover the range $3x10^{14}$ -$2.7x10^{15}$ cm^{-3}. The lowest densities were obtained by the PPP and PPP_QC followed by LSNS. Again the highest densities were obtained by QC_FFM and ZEST. For the P=2 bars case, PPP n°1 calculations gave the lowest density value followed by PPP n°2 and PPP_QC calculations with comparable values, QC_FFM gave an electron density about 5 times higher. For cases 14d-f, corresponding to P=3, 4, 5 bars, PPP gave electron densities again about 5 times lower than those given by QC_FFM. It is clear that these comparisons do not allow to determine the electron density with accuracy as its determination depends on many factors such as the retained broadening mechanisms and the temperatures of the electrons in addition of those of the ions and neutrals. It is clear that for low-temperature dense plasmas, accounting for neutral broadening is essential and any code which ignores it inevitably would overestimate the electron density to compensate for the missing van der Waals broadening in a way that the higher the pressure, the larger the mistake. These are not the only reasons explaining the large dispersion of the deduced electron densities since as we have seen even the pure Stark calculations differ for some unfavorable conditions like high electron densities and low temperatures. Further we concluded to the necessity of carrying out further analyses consisting in preferably fitting/analyzing the H-β line and He I 492 nm. Some papers submitted to this issue have started in this way to improve this spectroscopic diagnostic.

Acknowledgments: The work of E.S. was supported in part by the Israel Science Foundation.

Author Contributions: N. Bonifaci provided the experimental data. All authors contributed equally.

Conflicts of Interest: The authors declare no conflict of interest.

References

1. Stambulchik E., *Review of the 1st spectral line shapes in plasmas code comparison workshop*, High Energy Density Physics, **2013**, 9, 528.
2. See http://plasma-gate.weizmann.ac.il/projects/slsp/slsp4/ (version Feb. 22, 2018)
3. Rosato, J; Bufferand, H; Koubiti, M; Marandet ,Y; Stamm, R. *A table of Balmer γ line shapes for the diagnostic of magnetic fusion plasmas*. J. Quant. Spectrosc. Radiat. Transfer **2015**, 165, 102-107.
4. Stambulchik, E.; Maron, Y. A study of ion-dynamics and correlation effects for spectral line broadening in plasma: K-shell lines. J. Quant. Spectrosc. Radiat. Transf. **2006**, 99, 730–749.
5. Stambulchik, E.; Alexiou, S.; Griem, H.R.; Kepple, P.C. Stark broadening of high principal quantum number hydrogen Balmer lines in low-density laboratory plasmas. Phys. Rev. E Stat. Nonlin. Soft Matter Phys. **2007**, 75, 016401.

6. Calisti, A; Khelfaoui, F; Stamm, R; Talin, B; Lee, R. W. Model for the line shapes of complex ions in hot and dense plasmas. Phys. Rev. A **1990**, 42, 5433-5440.
7. Stambulchik, E; Maron, Y. Quasicontiguous frequency-fluctuation model for calculation of hydrogen and hydrogenlike Stark-broadened line shapes in plasmas. Phys. Rev. E **2013**, 87, 053108.
8. Gilleron, F; Pain, J.-C. ZEST : *a fast code for simulating Zeeman-Stark line-shape functions*. This issue.
9. Lee, R.W. *Plasma line shapes for selected transitions in Hydrogen-, Helium – and Lithium-like ions*. . J. Quant. Spectrosc. Radiat. Transfer **1988**, 40, 561-568.
10. Potekhin, A.; Chabrier, G.; Gilles D. Electric microfield distributions in electron-ion plasmas. Phys. Rev. E **2002**, 65, 036412.
11. Gilles, D.; Peyrusse, O. *Fast and accurate line shape modeling of the H- and He-like Lyman series for radiative transfer calculations in plasmas*. J. Quant. Spectrosc. Radiat. Transfer **1995**, 53, 647-661.
12. Calisti, A; Mossé, C; Ferri, S; Talin, B; Rosmej, F; Bureyeeva, L.A.; Lisitsa, V.S. Dynamic Stark broadening as the Dicke narrowing effect. Phys. Rev. E **2010**, 81, 016406.
13. Griem, H. R.; Blaha, M. and Kepple, P. C. *Stark-profile calculations for Lyman-series lines of one-electron ions in dense plasmas*. Phys. Rev. A **1979**, 19, 2421.
14. Li, Z.-L.; Bonifaci, N.; Aitken, F.; Denat, A.; von Haeften, K.; Atrazhev, V.M.; Shakhatov, V.A. *Spectroscopic investigation of liquid helium excited by a corona discharge: Evidence for bubbles and "red satellites"*. Eur. Phys. J. Appl. Phys. **2009**, 47, 2821.
15. Rosato, J.; Bonifaci, N.; Li, Z.; Stamm, R. Line shape modeling for the diagnostic of the electron density in a corona discharge. Atoms, **2017,** 5, 35.
16. Ali, A. W; Griem, H. R. *Theory of resonance broadening of spectral lines by atom-atom impacts*. Phys. Rev. **1965**, 4A, A1044.
17. Laux, C. O.; Spence, T. G.; Kruger, C. H. and Zare, R.N. *Optical diagnostics of atmospheric pressure air plasmas*. Plasma Sources Sci. Technol. **2003**, 12, 125-138.
18. Nikiforov, A. Yu.; Leys, Ch.; Gonzalez, M. A. and Walsh, J. L. *Electron density measurement in atmospheric pressure plasma jets: Stark broadening of hydrogenated and non-hydrogenated lines*. Plasma Sources Sci. Technol. **2015**, 24, 034001.
19. Yubero, C.; Dimitrijevic, M.S.; García, M.C.; Calzada, M.D. *Using the van der Waals broadening of the spectral atomic lines to measure the gas temperature of an argon microwave plasma at atmospheric pressure*. Spectrochim. Acta B **2007**, 62, 169–176.
20. Allard, N.; Kielkopf, J. *The effect of neutral non resonant collisions on atomic spectral lines*. Rev. Mod. Phys. **1982**, 54, 1103.
21. Muñoz, J.; Dimitrijevic, M.S.; Yubero, C.; Calzada, M.D. *Using the van der Waals broadening of spectral atomic lines to measure the gas temperature of an argon-helium microwave plasma at atmospheric pressure*. Spectrochim. Acta B **2009**, 64, 167–172.
22. Mossé, C; et al. *A new procedure to determine the plasma parameters from a genetic algorithm coupled with the spectral line shape PPP*. Atoms this issue.
23. Rosato, J; Bonifaci, N; Li, Z; Stamm, R. A spectroscopic diagnostic of the electron density in a corona discharge. J. Phys. Conf. Ser. **2017**, 810, 012057